Iranian Journal of Pharmaceutical Sciences
Spring 2008: 4(2): 163-168
www.ijps.ir

Original Article

Effect of Ultrasonic on Crystallinity of Nano-Hydroxyapatite via Wet Chemical Method

Sahebali Manafi*, Seyyed Hossein Badiee

Materials Engineering Department, Islamic Azad University-Shahrood Branch, Shahrood-Iran

Abstract

In a hydrothermal route devoted for synthesis of $Ca_{10}(PO_4)_6(OH)_2$ (HA) nanostructures, morphology can be controlled by experimental condition to form magical HA or nanostructured nanoparticles. In an intermediate condition, a novel nanostructure namely rose-like bundle of HA rod-likes was found, which is different from known HA nanostructures. The chemical synthesis of nanopowders under hydrothermal process provides an opportunity to control the HA and is dependent on sonochemical process. Since the procedure is very simple, this method is of general interest, and can be used for similar syntheses. The phase purity of the as-prepared products was determined by X-ray diffraction (XRD), fourier transform infrared (FT-IR), and scanning electron microscopy was applied to investigate the morphology. The microstructure of the HA products was further observed by transmission electron microscopy and energy-dispersive X-ray spectroscopy. The chemical composition of the as-synthesized powder was analyzed by inductively coupled plasma atomic emission spectroscopy. Interestingly, the approach proposed can be used for the preparation of different nanostructures of HA.

Keywords: Biocompatibility; Biomedical; Hydroxyapatite; Nanostructure.
Received: December 20, 2007; *Accepted:* March 14, 2008

1. Introduction

Systematic manipulation of morphology and architecture of inorganic crystals in microscale and nanoscale levels is a significant challenge, which attracts increasing attention because of their strong influence on material properties [1, 2]. For example, in the biomineralization process of vertebrate hard tissues, some specific molecules control the nucleation and growth of inorganic crystals (hydroxyapatite, $Ca_{10}(PO_4)_6(OH)_2$), resulting in the formation of hierarchical structure of teeth and bones with superior mechanical properties [3]. Thus, controlled syntheses of apatitic crystals with various morphologies have been the focus of intensive research out of the desire to more completely understand the biomineralization and utility in industrial and biomedical applications [4]. More recently, with the growing necessary of biomaterials, hydroxyapatites have received extensive attention [5-10]. So, researchers further placed

*Corresponding author: Sahebali Manafi, Materials Engineering Department, Islamic Azad University-Shahrood Branch, Shahrood-Iran, P.O. Box 36155-163.
Tel (+98)273-3334530, Fax (+98)273-3334537
E-mail: ali_manafi2005@yahoo.com

emphasis upon controlling the stoichiometric of the products, whereas with the development of nanotechnologies, considerable effort is now focused on controlling the morphology and size [11-13] because studies have shown that many clinical capabilities of hydroxyapatites mainly depend on their morphology and size [14]. Therefore, synthesis of nanoscale hydroxyapatite (HA) will largely improve their clinical applications. On the other hand, morphology of the HA is one of the most important factors on biocompatibility in the living tissue. Then, it is necessary to know the total effect of the various factors during hydrothermal-sonochemical synthesis on the morphology of the synthesized HA. Our present study is focused on the investigation of the effect of sonochemical time on morphology and the crystallinity of the synthesized compounds. HA powders can be synthesized by a variety of methods such as solid-state reaction, chemical precipitation and hydrothermal technique [15, 16]. Solid-state reactions usually give a stoichiometric and well-cryatallized product, but they require relatively high temperatures and long heat-treatment times. Moreover, the sintering ability of such powders is usually low and ultimately results in lower mechanical properties of the sintered matrixes [16]. In the case of chemical precipitation, nanometer-sized powders can be prepared. However, their crystallinity and Ca/P ratio depend mainly upon the preparation condition and are in many cases lower than for well-crystallized stoichiometric HA [16]. The hydrothermal technique usually gives HAp powders a high degree of crystallinty and a Ca/P ratio close to the stoichiometric value [16]. However, the obtained powders are usual in agglomeration and the size distribution is usual in the wide range. Therefore, the size distribution of HA powders can not be well controlled using a normal hydrothermal method. A newly developed sonochemically hydrothermal technique is used to synthesize nanopowders, nanoneedles and nanowires and this method is considered as an effective, convenient and facile synthetic methodology.

2. Materials and methods

The synthesis of stoichiometric HA nanopowders was performed in a 25 ml Teflon-lined stainless steel autoclave. All the reactants, $Ca(NO_3)_2$ (99% Merck), $(NH_4)_2HPO_4$ (99% Alfa), and NaOH (96% Aldrich), were of reagent grade and used without further purification. In a typical

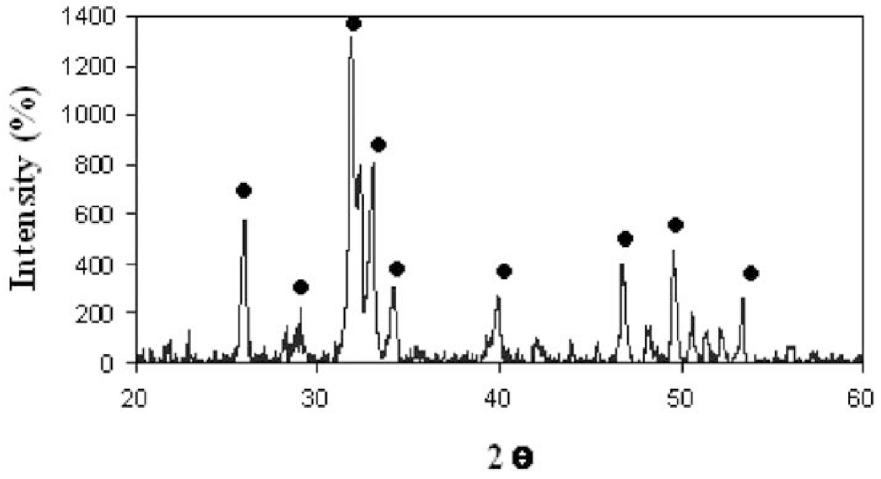

Figure 1. XRD patterns of HA samples.

experiment, a solution was first prepared by dissolving $Ca(NO_3)_2$ and $(NH_4)_2HPO_4$ and distilled water in amounts corresponding to the molar ratio of calcium to phosphorous of 1.67. Subsequently, some NaOH was added to the solution to keep its pH around 10. Before being tranferred to a Teflon-lined autoclave, the solution mixture was pretreated under an ultrasonic water bath for different times (30, 60, 90, and 120 min.). The hydrothermal syntheses were conducted at 150 °C for 24 h in an electric oven. After the reaction, crystalline products of HA were harvested by centrifugation and through washings with deionized water. The obtained HA nanorods were characterized with scanning electron microscopy, energy-dispersive X-ray spectroscopy (SEM/EDX, XL30), and transmission electron microscopy (TEM). The size distribution and morphology of the samples were analyzed by field emission gun (FEG) transmission electron microscope, selected area electron diffraction (TEM/SAED) observation on a Philips CM200 transmission electron microscope operated at 200 kV. X-ray diffraction patterns were recorded in the angular range 2θ=20-60º. For these experiments, a Siemens diffractometer (30 kV and 25 mA) with the $K_{\alpha 1}$, radiation of copper (λ=1.5406 Å), was used. The powder product was further investigated using Fourier transform infrared (FT-IR) spectroscopy in a Bruker-IR spectrometer from 500 to 4000 cm^{-1} using the KBr technique and operating in the transmittance mode. The crystallite size of the powder was evaluated from the peak broadening of XRD patterns based on Scherrer's formula as Equation (1) [17]:

$$D = \frac{0.9\,\lambda}{FWHM.Cos\theta} \qquad \text{Equation (1)}$$

in which D is the crystallite size (nm), λ is the wavelength of the monochromatic X-ray beam (λ=0.154056 nm for CuKα radiation), FWHM is the full width at half-maximum for the diffraction peak under consideration (rad), and θ is the diffraction angle (deg).

3. Results and discussion

On the basis of the XRD results (Figure 1), the crystallographic phase of these different HA nanopowders belongs to the wurtzite-type (space group: $P6_3/m$), and the measured lattice constants of c_0 and a_0 of this hexagonal phase are 6.88 and 9.42 Å, respectively. Althogth the majority of HA nanorods were assembled into the bush-like aggregates (Figure 1), individual nanorods can be separated with sonication. So, the XRD patterns in Figure 1 correspond to products with the initial Ca:P molar ratio of 5:3 obtained at 150 °C for 24 h. All peaks of the products can be indexed to stoichiometric HA composition with hexagonal structure. No tri-calcium phosphate (TCP) and other impurity phases are detected. The strong and sharp peaks and very low backgrounds reveal that the as-synthesized HAp nanoparticles

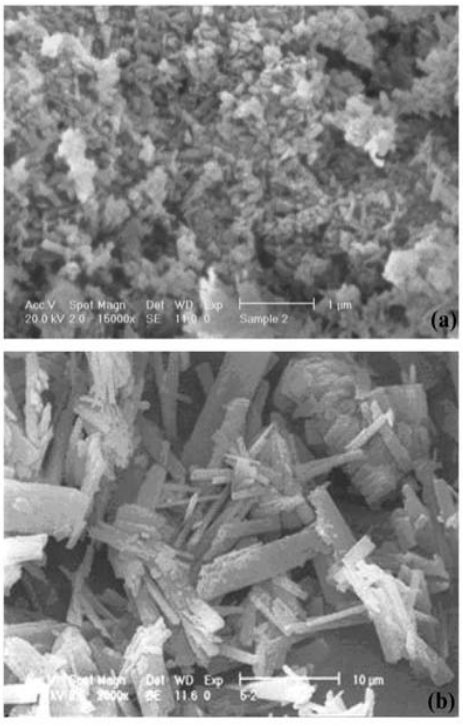

Figure 2. SEM images of hydroxyapatite samples at different sonochemical time (a): 0 min.; (b): 30 min.

had a high degree of crystallinity. The broading of the diffraction peaks indicates that the samples are nanosize.

Figure 2 shows SEM images of two HA samples prepared under hydrothermal process with different holding times in the autoclave, for 30 and 60 min., respectively. Severe structural changes of the HA morphology are obvious. The efficincy of this approach for controlling the morphology is due to the fact that there is a systematic relationship between the morphology of the HA microstructure and the residence time in the autoclave. On the other hand, the morphology changes by increasing the sonochemical time. For the sonochemical sample for 30 min., after hydrothermal synthesis the HA has a uniform nanostructure (Figure 2). Alternatively, we focused on the synthesis and inspected even tiny changes in the experimental conditions. As a result, we found an interesting nanostructure as an intermediate in the structural transition form nanoparticle to rod-like nanostructure by changing initial sonochemical time from 30 min. to 60 min. When the HA nanoparticle is generated without sonochemical (Figure 2a) while with sonochemical time for 30 min., HA rod-like structures are formed (Figure 2b), which tend to uniform rod-like structure with ultra-high crystalinity with sonochemical time.

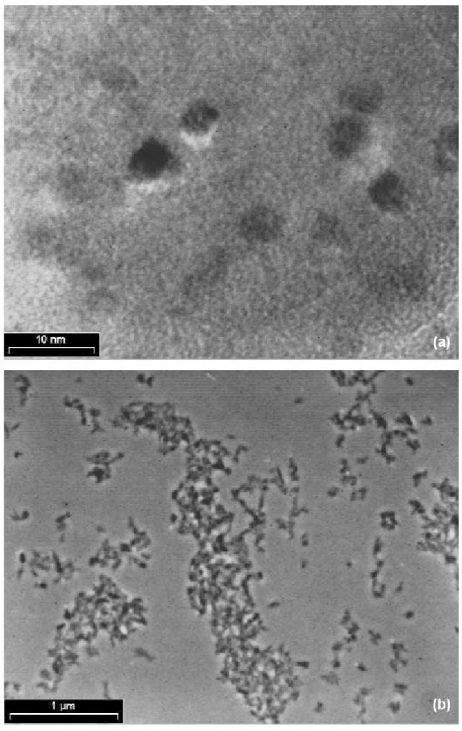

Figure 3. TEM images of HA samples at different sonochemical time (a): 0 min; (b): 30 min.

At the same time, these results are consistent with the HRTEM image observations. Figure 3 reveals the morphology of nanoparticles formed at 150 °C for 24 h, while being transferred to a Teflon-lined autoclave, the solution mixture was pretreated under an ultrasonic water bath for 30 min. Figure 3a shows the morphology of nanopartiles obtained at 150 °C for 24 h (without the pressure of ultrasonic irradiation) revealing 20-30 nm apherical particles, in agreement with the sizes calculated by using the Scherrer formula. Figure 3b shows nanoparticles whose diameter are 70-100 nm and length 70-150 nm, obtained at 150 °C for 24 h, with 30 min. ultrasonic irradiation. It is quite obvious that the morphologies of the products change considerably as a function of the residence time in the autoclave. On the basis of the morphologies observed by TEM, it can be concluded that the sizes of the particles increase with the increase of ultrasonic time in autoclave stage, a fact that is consistent with the results of the patterns.

The SAED pattern shows from the as-prepared HA nanostructure synthesized at 150 °C for 24 h consists of a number of rectangular and some distinct spots along the ring contours, suggesting a hexagonal structure (not shown). The apots in an electron diffraction pattern arise due to the diffracted electron beam from a set of lattice planes in the crystallines present in the sample satisfying the Bragg diffraction condition. In other words, the ring is an envelope of all diffracted apot. Among same of the rings a few spots appear to be prominent, which

indicates the formation of crystallines. The interplanar spacing values are calculated from Bragg's diffraction equation using the diffraction ring diameter and the camera length of the transmission electron microscopy (TEM).

The chemical stoichiometry of nanorods was investigated with EDX (Figure 4) which indeed gave an atomic ratio of HA~1.67. At the same time, this result is consistent with the inductively coupled plasma (ICP) calculation. More details about the structure of HA nanostructures were investigated by the SAED pattern and high resolution transmission microscopy (HRTEM).

Fourier transform infrared (FT-IR) analysis revealed the presence of carbonate on the surface of the HA. Figure 5 shows the transmittance infrared spectrum of synthetic HA in the 4000-650 cm^{-1} region. A narrow band located near 965 cm^{-1} (962 cm^{-1} in Figure 5) represents the υ_1 mode of PO_4^{3-} ions in apatite. The main signal of phosphate appears in the triply degenerate υ_3 domain (1000-1100 cm^{-1}). The adsorption band at 3500 cm^{-1} confirmed the presence of OH^- groups. The υ_2 peak of CO_3^{2-} is located at 875 cm^{-1}; this absorption results from out-of plane stretching. The υ_3 mode, near 1400 cm^{-1}, is the strongest IR peak for carbonate. This peak is actually composed of two bands (1421 cm^{-1}, in Figure 5) [18, 19]. The shape of the υ_3 signal and the absence of the C-O absorption bands at 700 cm^{-1} indicate that no calcite was associated with the HA. Carbonate ions can substitute for either OH^- or PO_4^{3-} ions in the apatite structure (type A CO_3^{2-} or type B CO_3^{2-}) [20].

4. Conclusion

In summary, an effective method was developed for the formation of ultra-crystallinity rod-like HA. The nano-rods are highly aspect-ratio, crystalline and uniformly structured. These high-quality HA nano-rods represent well-defined nanoscale structure needed for both fundamental studies and clinical applications. As the matter of fact, this method (hydrothermal synthesis) guarantees its production in the synthesis of HAs for different morphologies.

5. Acknowledgments

The author thanks the Tarbit Modarres University for access to SEM and technical support. So, the author would like to acknowledge Dr. Hesari for investigating TEM image, Mr. Nouri for helping in preparing of this paper and Mr. Jabbari for performing the experimental tests.

References

[1] Beall GH, Chyung K, Watkins HJ. Fluormica glass-ceramics. *US Patent US-PS* 1974; 3,801,295, Apr. 2.

[2] Vogel W, Holand W, Naumann K, Gummel JJ.

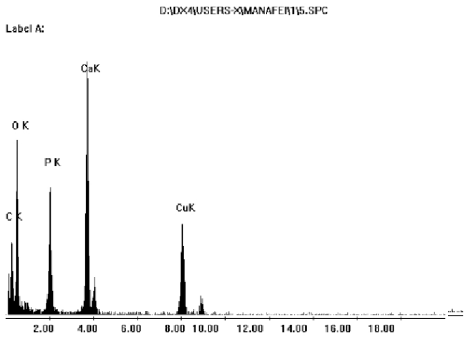

Figure 4. EDAX of the obtained HA products.

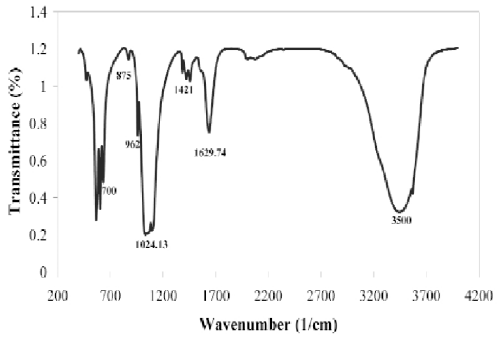

Figure 5. The FTIR spectrum of the HA nanostructures.

Development of machineable bioactive glass ceramics for medical uses. *Non-Cryst Solids* 1986; 80: 34-51.

[3] Hill R, Wood DJ. Apatite-mullite glass-ceramics. *Mater Sci Mater Med* 1995; 6: 311-8.

[4] Muller R, Abu-Hilal LA, Reinsch S, Holand W. Coarsening of needle-shaped apatite crystals in $SiO_2.Al_2O_3.Na_2O.K_2O.CaO.P_2O_5.F$ glass. *J Mater Sci* 1999; 34: 65-9.

[5] Rey C. Calcium phosphate for medical applications. In: Amjad Z, (editor). *Calcium phosphate in biological and industrial systems*. Boston: Kluwer Academic Publishers, 1998; p. 217.

[6] LeGeros RZ. Calcium phosphates in oral biology and medicine. *Monographs in Oral Science* 1991; p. 15.

[7] Elliott JC. Structure and chemistry of the apatites and other calcium orthophosphates. Amsterdam: Elsevier, 1994.

[8] De Groot K. *Bioceramics of calcium phosphate.* Boca Raton: CRC Press, 1983; p.100.

[9] Aoki H. *Medical applications of hydroxyapatite*. Tokyo: Ishiyaku Euroamerica, Inc., 1994.

[10] Van Raemdock W, Ducheine P, De Meester P. Calcium phosphate ceramics. In: Ducheine P, Hastings H, (editors). *Metal and ceramic biomaterials*. Vol. 2. Boca Raton: CRC Press, 1984.

[11] Rodrrguez-Lorenzo LM, Vallet-Regr M. Controlled crystallization of calcium phosphate apatites. *Chem Mater* 2000; 12: 2460-5.

[12] Hirai T, Hodono M, Komasawa I. The preparation of spherical calcium phosphate fine particles using an emulsion liquid membrane system. *Langmuir* 2000; 16: 955-60.

[13] Yuan ZY, Liu JQ, Peng LM. Morphosynthesis of vesicular mesostructured calcium phosphate under electron irradiation. *Langmuir* 2002; 18: 2450-2.

[14] Elliott JC. Recent studies of apatites and other calcium orthophospates. In: Bres E, Hardouin P, (editors). *Calcium phosphate materials, fundamentals*. Monpellier: Sauramps Medical, 1998; p. 25.

[15] Elliott JC. *Structure and chemistry of the apatites and other calcium orthophosphates*. Amsterdam: Elsevier, 1994.

[16] Byrappa K, Yoshimura M. *Handbook of hydrothermal technology*. Norwich: Noyes Publications/William Andrew Publishing, 2001.

[17] Landi SE, Tampieri A, Celotti G, Sprio S. Densification behaviour and mechanisms of synthetic hydroxyapatites. *J Eur Ceram Soc* 2000; 20: 2377-87.

[18] Doi Y, Moriwaki Y, Aoba T, Takahashi J, Joshin K. ESR and IR staudies of carbonate-containing hydroxyapatites. *Calcif Tissue Int* 1982; 34:178-81.

[19] Reigner P, Lasaga AC, Berner RA, Han OH, Zilm KW. Mechanism of CO_2^{-3} substitution in carbonate-fluorapatite: Evidence from FTIR spectroscopy, 13C NMR, and quantum mechanical calculations. *Am Mineral* 1994: 79; 809-18.

[20] Elliot J C. *Ph.D. Thesis*. London: University of London, 1964.